


Equivalence between pressure- and structure-defined ionization in hot dense carbonJean Cl  rouin ^{1,2} Augustin Blanchet ^{1,2} Christophe Blancard,^{1,2} G  rald Faussurier,^{1,2} Fran  ois Soubiran ^{1,2} and Mandy Bethkenhagen ³¹CEA-DAM-DIF, F-91297 Arpajon, France²Universit   Paris-Saclay, CEA, Laboratoire Mati  re sous conditions extr  mes, 91680 Bruy  res-le-Ch  tel, France³CNRS,   cole Normale Sup  rieure de Lyon, Laboratoire de G  ologie de Lyon LGLTPE UMR 5276, Centre Blaise Pascal, 46 all  e d'Italie Lyon 69364, France

(Received 23 June 2022; accepted 23 September 2022; published 19 October 2022)

The determination of the ionization of a system in the hot dense regime is a long standing issue. Recent studies have shown inconsistencies between standard predictions using average atom models and evaluations deduced from electronic transport properties computed with quantum molecular dynamics simulations [Bethkenhagen *et al.*, *Phys. Rev. Res.* **2**, 023260 (2020)]. Here, we propose a definition of the ionization based on its effect on the plasma structure as given by the pair distribution function (PDF), and on the concept of effective one-component plasma (eOCP). We also introduce a definition based on the total pressure and on a modelization of the electronic pressure. We show the equivalence of these definitions on two studies of carbon along the 100 eV isotherm and the 10 g/cm³ isochor. Simulations along the 100 eV isotherm are obtained with the newly implemented EXT. First principles molecular dynamics (FPMD) method in ABINIT for densities ranging from 1 to 500 g/cm³ and along the 10 g/cm³ isochor with the recently published Spectral quadrature DFT (SQDFT) simulations, between 8 and 860 eV. The resulting ionizations are compared to the predictions of the average-atom code QAAM which is based on the muffin-tin approximation. A disagreement between the eOCP and the actual PDFs (non-OCP behavior) is interpreted as the onset of bonding in the system.

DOI: [10.1103/PhysRevE.106.045204](https://doi.org/10.1103/PhysRevE.106.045204)**I. INTRODUCTION**

The ionization in a hot dense matter system is a quantity of fundamental interest since it drives the thermodynamic properties such as the pressure and the electronic properties such as conductivity or reflectivity. Recent experiments in the Gbar regime, have shown the crucial role of the ionization of inner atomic states in the compressibility of carbon [1]. However, since the ionization does not correspond to a quantum observable, it cannot be measured directly and its evaluation remains subject of discussions. Let us mention the experiments using pulsed electrical discharges on metallic wires that allowed first evaluations of the ionizations in the eV-kbar region through the measurement of the electrical conductivity [2,3].

Usually, the ionization is a byproduct of average atom (AA) codes, solving the Schr  dinger, or the Dirac equation for a single atom in a box. In a multicenter three dimensional density functional theory (DFT) resolution with the Kohn-Sham *ansatz* (KS-DFT), such as in ABINIT [4], there is no simple way to determine a number of free electrons per atom, since we only know the global electronic density, shared by the whole system. Driver *et al.* provided an approximation based on the integrated density of states [5]. More recently, the ionization has been estimated from the electrical conductivity computed from a Kubo-Greenwood formulation, using the concept of valence and conduction electrons with the associated sum rules [6]. This approach shows significantly higher ionization than the one given by an AA code such as PURGATORIO [7], by 20% in average. This work has triggered

new studies using various AA models such as the Quantum Average Atom Model (QAAM) [8] or the neutral pseudoatom (NPA-HNC) model [9], for which the ionization is directly deduced from the electronic description. To our knowledge there are no simple approaches allowing for a direct evaluation of the average ionization from a Quantum Molecular Dynamics (QMD) simulation (the molecular dynamics version of a KS-DFT or density matrix resolution of the N-body problem). There is also no unique definition of the ionization making it a difficult concept to grasp. For hot dense systems, the pressure, which is a straightforward product of QMD simulations, is nevertheless a signature of the mean ionization. The structure of the plasma, as given by the ion-ion pair distribution function (PDF), is another manifestation of the average ionization, through the effective charge of ions.

Whether along the 100 eV isotherm or the 10 g/cm³ isochor, carbon crosses regions with very different properties. They can be characterized by the coupling of the ions, and the degeneracy of the electrons. Note that both quantities involve the average ionization or the mean ionization state [10], we refer to Q to make a clear distinction with the atomic number Z ($0 \leq Q \leq Z$), being aware that this denomination remains elusive in some cases.

The behavior of the ions is characterized by the ionic coupling parameter, the ratio of the average potential energy to the kinetic energy. In atomic units, $\Gamma = Q^2/aT$, where a is the Wigner-Seitz radius $a = (3/4\pi n)^{1/3}/a_B$, a_B the Bohr radius, and n the ionic density. T is the ionic temperature (in Hartree) and Q is the mean ionic charge which depends

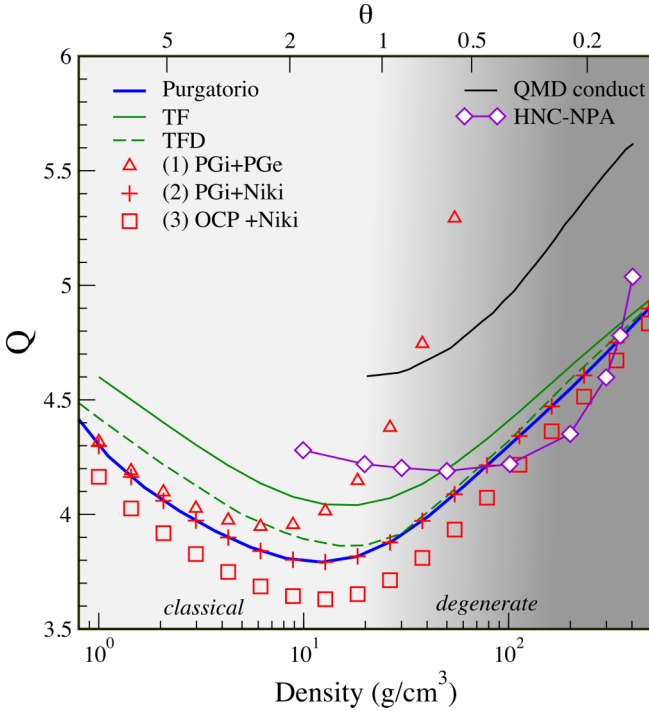


FIG. 1. Ionizations versus density from average-atom theories along the 100 eV carbon isotherm. Blue solid line: PURGATORIO, green solid line: TF, green dashed line: TFD. The solid black line is the conductivity ionization [6]. Symbols are the charge computed from the PURGATORIO pressure with option (1): red triangles; option (2): red crosses, and option (3): red squares. The corresponding degeneracy parameter θ , computed with an average ionization of 4, is shown on the upper x axis. The solid black line shows the ionization deduced from the conductivity [6], and the solid violet line with diamonds the NPA-HNC evaluation [9].

on the electronic temperature T_e . For simple systems, such as the one component plasma (OCP), the knowledge of this parameter allows for a complete description of the system (thermodynamic [11], structure [12] and transport [13]).

The quantum character of the electrons, the degeneracy, is measured by $\theta = T_e/T_F$, ratio of the electronic temperature to the Fermi temperature ($k_B T_F = 1/2(3\pi^2 n_e)^{2/3}$, with $n_e = Qn$,

and k_B the Boltzmann constant). This parameter, computed for an average ionization of 4, is displayed in Fig. 1 (upper scales) and reported in the third column of Tables I and II. Along the 100 eV carbon isotherm, in the Gigabar regime (100 TPa), the system transits from a kinetic regime at low density ($\theta \gg 1$), where the thermally activated ionization is described by the Saha equations (left side of Fig. 1) to a degenerate system at high density ($\theta \ll 1$), where the ionization results from orbitals overlap (right side of Fig. 1). At contrast, along an isochor, the system which is partially degenerate at low temperature, becomes more and more classical at high temperature. Along the isotherm, the minimum of ionization occurs in the vicinity of $\theta = 1$, which corresponds to the transition between the two regimes. Such a transition between a degenerate system to a classical one has been recently observed for deuterium by a reflectivity measurement on the Omega laser [14].

Also given in the fourth column of Tables I and II, the finite temperature inverse screening length as fitted by [15], which interpolates between the Thomas-Fermi result in the degenerate regime, and the Debye-Hückel result in the classical region. Along the 100 eV isotherm (Table I), κ is of order of the unity and almost constant. Along the 10 g/cm³ isochor (Table II) κ decreases from 2 to 0.5 with increasing temperature.

The aim of this paper is to show the equivalence of the ionization deduced from the pressure Q_P and the ionization Q_S deduced from the ionic structure. After reviewing recent results on carbon ionization, we establish a simple model to compute the ionization Q_P for a given pressure. This formulation is tested against pressures given by the PURGATORIO model. We then introduce the evaluation of the ionization by the structure Q_S by matching the PDF to the OCP one. These two independent evaluations are tested along the 100 eV carbon isotherm from EXT. First principles molecular dynamics (FPMD) simulations for densities ranging from 1 to 500 g/cm³, and along the 10 g/cm³ carbon isochore from Spectral quadrature DFT (SQDFT) simulations [16] for temperatures ranging from 0.1 to 10 MK. These evaluations are eventually compared to the predictions of the average atom code QAAM [8]. Finally, taking advantage of the equivalence of these two definitions, we build a non-OCP behavior parameter which is

TABLE I. Properties of carbon along the 100 eV isotherm from EXT. FPMD simulations. For each density, we give the Wigner-Seitz radius a in atomic units, the degeneracy parameter θ , the finite temperature inverse screening length κa , the number of orbitals needed for a 64 carbon atoms system and for a minimum occupation of 10^{-4} , the pressure in 10^2 GPa (Mbar), the effective coupling parameter Γ , the ionizations Q_S and Q_P , and the pressure coupling parameter Γ_P (see Sec. VII).

ρ g/cm ³	a a_B	θ	κa	$N_{\text{KS-DFT}}$	P 10 ² GPa	Γ	Q_S	Q_P	Γ_P
1	3.180	7.6	1.05	48100	41.5	1.6	4.30	4.15	1.5
2	2.524	5.1	1.13	28160	79.5	1.7	3.97	3.92	1.7
5	1.859	2.8	1.27	13600	191.4	2.1	3.79	3.69	2.0
10	1.476	1.8	1.37	7680	383.1	2.4	3.61	3.62	2.4
20	1.171	1.1	1.50	4352	804	3.2	3.71	3.67	3.1
50	0.863	0.6	1.57	2048	2376	4.8	3.90	3.92	4.8
100	0.685	0.4	1.54	1280	6063	7.0	4.20	4.19	7.0
200	0.544	0.2	1.44	768	17142	10	4.47	4.45	9.9
500	0.401	0.1	1.30	576	76508	17	5.00	4.79	15.6

TABLE II. Properties of carbon along the 10 g/cm^3 isochor ($a = 1.476 a_B$) from SQDFT simulations. For each temperature, we give the degeneracy parameter θ , the finite temperature inverse screening length κa , the pressure in 10^2 GPa (Mbars), the effective coupling parameter Γ , the ionizations Q_S and Q_P , and the pressure coupling parameter Γ_P (see Sec. VII).

T MK	T eV	θ	κa	P 10^2 GPa	Γ	Q_S	Q_P	Γ_P
0.1	8.62	0.20	2.17	43.46	14	2.56	2.37	12.0
0.2	17.24	0.38	2.09	69.30	8	2.74	2.63	7.4
0.5	43.10	0.89	1.77	157.7	4	3.06	3.12	4.2
0.75	64.65	1.28	1.57	238.8	3	3.24	3.34	3.2
1	86.2	1.65	1.43	330.0	2.5	3.42	3.58	2.7
2	172.4	2.82	1.16	771.6	2.0	4.33	4.47	2.1
5	431.0	6.17	0.82	2260.0	1.2	5.30	5.50	1.3
10	862.0	11.72	0.61	4722.2	0.7	5.72	5.81	0.7

related to the onset of binding structures in the carbon plasma. The EXT, FPMD, SQDFT, and QAAM models are described in Appendices A, B, and C, respectively.

II. AVERAGE ATOM PREDICTIONS

A straightforward way to get insight on the ionization is to solve the radial Thomas-Fermi (TF) equation for one atom in a box representative of the density, and to compute the radial distribution of the electronic density. Here we face a first choice for defining the ionization: do we take the electronic density at the edge or the electronic states with positive energy? These two definitions differ, in general by 10%, and are notoriously wrong at low density and/or at low temperature. Adding a Dirac exchange correction (TFD), improves the prediction at low temperature.

A more accurate approach is brought by a full quantum-mechanical resolution of an AA model such as PURGATORIO [7], TARTARUS [17], atoMEC [18], QAAM [8], AVION [19], and the neutral pseudoatom (NPA-HNC) model [9], where for the latter a ionic structure is incorporated. The points of the NPA-HNC model also show that the introduction of an ionic structure in an AA model, by a Hyper-netted chains (HNC) calculation, or a variational estimation using hard spheres or OCP, does not always improve the prediction, as we noted with the SCAALP model [20,21].

Let us mention also the models based on Saha-Boltzmann equations that can be coupled to collisional-radiative models to produce opacities and a detailed description of the ionic composition [22]. These models, are limited in density, and also need the computation of atomic data and ionization potential depression; thus introducing additional parameters.

We present in Fig. 1 a comparison of the ionizations predicted by a selection of AA models. The green solid line and the green dashed line are, respectively, the TF and TFD ionizations. The blue heavy curve is the PURGATORIO curve reported in Ref. [6], the solid black line is the ionization computed from the conductivity [6], and the solid violet line with diamonds is the NPA-HNC evaluation [9]. One can see that a simple TFD prediction is very close to PURGATORIO at low density, but the conductivity evaluation is higher by about 20%.

III. THE IONIZATION FROM THE PRESSURE

One of the most obvious effects of the ionization is to drive the total pressure. For hot and dilute systems (kinetic regime) the pressure is given by

$$P = (Q + 1)k_B T, \quad (1)$$

where T is the temperature and k_B the Boltzman constant. This perfect gas (PG) formulation is no longer true for dense systems, when the Fermi degenerate pressure overtakes the kinetic pressure. Along isotherms the electron statistics transits from a kinetic regime ($P \propto T$), at low density, to a degenerate regime, at high density, where the pressure only depends on the electronic density ($P \propto n_e^{5/3}$).

A formulation due to Nikiforov [23] interpolates between these two regimes for the electronic pressure of the homogeneous electron gas,

$$\frac{P_{\text{ele}}}{n_e k_B T} = \frac{1}{k_B T} \left[(k_B T)^3 + 3.36 n_e (k_B T)^{3/2} + \frac{9\pi^4}{125} n_e^2 \right]^{1/3}, \quad (2)$$

where n_e was previously defined.

A similar change occurs for the ions along an isotherm, transiting from a kinetic regime at low density to a strongly coupled regime at high density. The OCP formulation [11] of the pressure describes this transition

$$\frac{P_{\text{OCP}}}{n k_B T} = 1 + \frac{1}{3} [0.94544 \Gamma^{1/4} + 0.17954 \Gamma^{-1/4} - 0.80049], \quad (3)$$

where the first term -0.89752Γ , which corresponds to the lattice energy, has been omitted.

In order to test these different options we have used the fit given by Faussurier *et al.* [8], that reproduces the total pressure P_{AA} computed by the AA code QAAM in perfect agreement with PURGATORIO. To deduce the ionization Q from the total pressure P_{AA} , three options can be considered:

Option 1: Both ion and electron contributions to the pressure are given by the perfect gas:

$$P_Q = P_{\text{PG}}^i + P_{\text{PG}}^e$$

Option 2: The ion pressure is given by the perfect gas and the electron pressure by the Nikiforov interpolation formula (2):

$$P_Q = P_{\text{PG}}^i + P_{\text{Niki}}^e.$$

Option 3: The ion pressure is given by the OCP model (3) and the electron pressure by the interpolation (2):

$$P_Q = P_{\text{OCP}}^i + P_{\text{Niki}}^e.$$

We then search for the mean ionization Q that gives a difference $P_{\text{AA}} - P_Q$ smaller than a given precision, with the previous options 1, 2 or 3 for computing P_Q . A secant algorithm is used to this end starting from two estimations bracketing the solution: the Thomas-Fermi Q_{TF} estimation that overestimates the ionization and a lower bound $Q_{\text{TF}} - 20\%$ that underestimates the ionization. Convergence is quickly reached, and the corresponding ionic charges versus density are represented by symbols in Fig. 1 for the three options.

The red triangles correspond to the option (1): fully kinetic pressure. It quickly goes wrong as soon as the first degeneracy effects appear. Squares correspond to option (3) and underestimate the ionization by 5%. The best agreement with PURGATORIO prediction is obtained with option (2), where the pressure of the ions is given by the perfect gas and electron pressure by the Nikiforov interpolation formula. This is not surprising since, in AA and QMD codes, the total pressure is given by an electronic contribution to which a perfect gas contribution for the ions is added. To infer the ionizations from the pressures obtained along isotherm or isochor we will thus use option (2).

We emphasize that our estimation of the electronic pressure is valid in the kinetic regime but also in the degenerate regime.

IV. THE IONIZATION FROM THE STRUCTURE

We propose an alternative route provided by the effect of the ionization on the ionic structure, which is given by the ionic PDF, a standard output of molecular dynamics simulations. The ionic structure reflects the electronic distribution (bound and free states). If the electrons are at a higher temperature than the ions, the extra ionization results in a more structured PDF (see, e.g., Refs. [24,25]). It is known that, at sufficiently high temperature, the PDF of any pure element, can be matched by standard OCP results that depends only in the coupling parameter Γ , defining an effective OCP (eOCP) plasma [26–29]. This matching is not perfect, and screening effects are evidenced by the computation of the static structure factor (SSF). The limit of the SSF of the real system at vanishing $q = ka$ is finite and gives the compressibility, when the one of the eOCP is zero ($q^2/3\Gamma$). In other words, screening appears at long distance and eOCP is meaningful at short distances [30]. At short distances, an analytical formulation made by Ott *et al.* [31], provides a link between the structure of the PDF at half height and the coupling strength. The leading eOCP effective coupling parameter Γ gives an ionization

$$Q_S = \sqrt{\Gamma a T}, \quad (4)$$

where Q_S , a , and T are expressed in atomic units. For a given PDF, we searched for the best agreement between QMD and the OCP one, by varying the coupling parameter. To generate the OCP PDFs we used the parametrization [12].

One could ask why not prefer a Yukawa-based functional? The answer is twofold: first, neglecting screening and (arbitrary) short-range repulsion allows for a simple one parameter optimization. Second, to our knowledge, there are no sim-

ple analytical PDF generators for Yukawa systems. We have tested that our effective OCP approach describes Yukawa systems with enough accuracy [32].

The accuracy of the method can be evaluated by differentiating the expression (4)

$$dQ_S = \frac{1}{2} \sqrt{\frac{aT}{\Gamma}} d\Gamma, \quad (5)$$

which in relative errors gives $dQ_S/Q_S = 0.5d\Gamma/\Gamma$. A variation of 10% of the effective coupling Γ translates into an error of 5% in the ionization.

V. IONIZATION ALONG AN ISOTHERM

We performed EXT. FPMD simulations of carbon at 100 eV and for densities of 1, 2, 5, 10, 20, 50, 100, 200, and 500 g/cm³ with 64 atoms, and with a total number of 500 orbitals only instead of the recommended number for conventional KS-DFT calculations given in column 5 of Table I. The Perdew-Burke-Ernzerhof exchange correlation [34] was used. We designed special all electrons projected augmented wave (PAW) pseudopotential with the ATOMPAW code [35] with a small augmentation radius (0.3 Bohr) to accommodate the high densities, with a cutoff energy of 200 Hartree. Compared to WIEN2k [36], our pseudopotential gave a Delta factor [37] of 0.8 meV/at on the cold curve. We checked that for the highest density (500 g/cm³), the overlap occurrences were never higher than 10%. We took advantage of the method to run longer simulations with a significant number of particles and to get more accurate PDFs. Up to 10 000 time steps of 1 atomic unit were produced, from which we discarded the first 1 000 time steps. We used an isokinetic algorithm which is reliable for static quantities.

The comparison of the EXT. FPMD PDFs (open black circles) with the OCP one (heavy solid red lines) is shown in Fig. 2(a). At low density (1–5 g/cm³) this eOCP concept works very well, since electrons are fully kinetic and are not polarized by the ions providing an excellent agreement between simulations and eOCP. On the other side, at high density (500 g/cm³), the electrons start being degenerate, allowing for a sound eOCP description. At intermediate density (10–50 g/cm³) the agreement is less good since the PDF exhibits a slight bump between 1–1.5 (in a units) that cannot be reproduced by the eOCP model. Since the eOCP model involves purely repulsive interactions, we believe that this bump signals the onset of binding leading to complex structures. In this case we concentrated on the closest approach distance (the feet) and on the value for $g(r) = 0.5$ in the matching procedure.

The SSF obtained, for each density, by Fourier transforming the PDFs are shown in Fig. 2(b) (open black circles). The previous eOCP coupling parameters are used to produce eOCP SSF (heavy solid red lines) using the same analytical generators. The general agreement is excellent [38], except at low q where the SSF of the simulations goes to a finite value when the eOCP one goes to zero as $q^2/3\Gamma$. This is a manifestation of screening we have neglected in real space at short distance, and can be corrected at low q by the expansion $(q^2 + \kappa^2)/(q^2 + \kappa^2 + 3\Gamma)$ shown by the heavy blue line in Fig. 2(b) for each temperature. The corresponding inverse

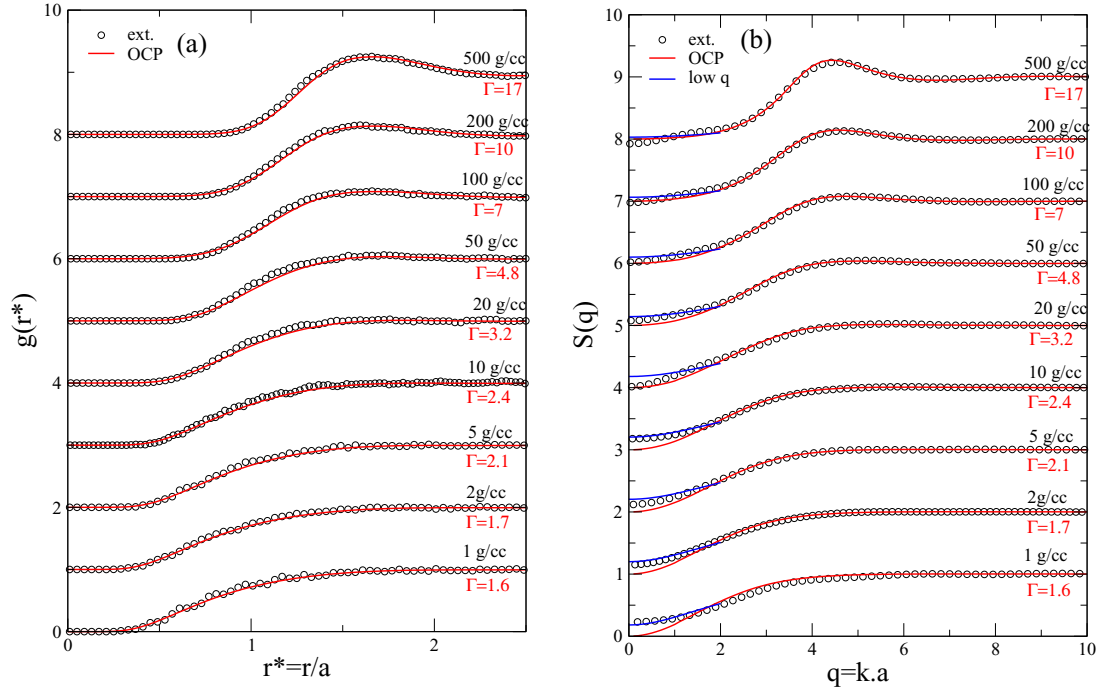


FIG. 2. PDF (a) and static structure factor (b) of carbon along the 100 eV isotherm, and for densities of 1, 2, 5, 10, 20, 50, 100, 200, and 500 g/cm³ computed with the EXT. FPMD simulations (open black circles) and matched with the OCP one (heavy red line). The blue line in (b) is the low q expansion of the SSF for screened systems.

screening lengths, κ , are given in Table I. As shown before [30], screening appears at low q (long distance) when at short distance the eOCP model (without screening) is relevant.

The effective coupling parameters and the resulting structure ionizations Q_S are given in Table I and are reported in Fig. 3. The pressures were averaged from the EXT. FPMD simulations after the equilibration phase and with a statistical error of about 1%. They are reported in Table I, and found in average 3–4% lower than the PURGATORIO results, resulting in lower ionizations Q_P by the same amount (see Fig. 3). One can first acknowledge the coherency of the two approaches, pressure and structure.

To ensure the validity of our findings, we compare in Fig. 4(a) the structure obtained with the EXT. FPMD model at 10, 50, and 200 g/cm³ and 100 eV with the one resulting in an average-atom code coupled with an HNC calculation (the NPA-HNC model [9]). We observe an excellent agreement for the two lowest densities (10 and 50 g/cm³), but for the highest density (200 g/cm³), our PDF appears slightly more structured than the HNC result ($\Gamma = 10$ instead of 8). This discrepancy can be attributed to a well-known tendency of HNC to underestimate the structure at strong coupling. The effective OCP result is close to the previous data but is always a little bit off in the region $0.75 < r/a < 1.5$. Although the PDFs are very close, the ionizations deduced from these different models are quite different in the transition zone ($\theta \simeq 1$) as shown by the violet line with diamonds in Fig. 1; which we cannot explain.

Q_S and Q_P are also in good agreement with AA estimations such as PURGATORIO [7] or QAAM [8], which suggests that an estimation based on the electrical conductivity may be biased by the well-known underestimation of the gap of carbon with KS-DFT techniques. It must be noted that QAAM and PURGATORIO, which are pure average atom codes, are in

excellent agreement. The larger differences between the various models are observed for an intermediate density of about 10 g/cm³ which corresponds to the transition between the

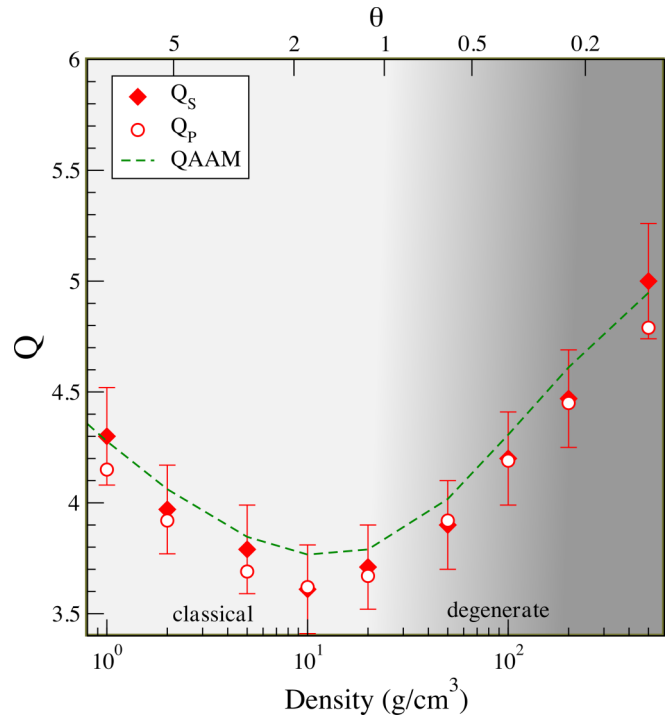


FIG. 3. Ionization versus density along the 100 eV carbon isotherm. Red diamonds with errors bars are the structure estimation Q_S , and red circles the pressure estimation Q_P , both from EXT. FPMD simulations. The green dashed line is the QAAM estimation. [8].

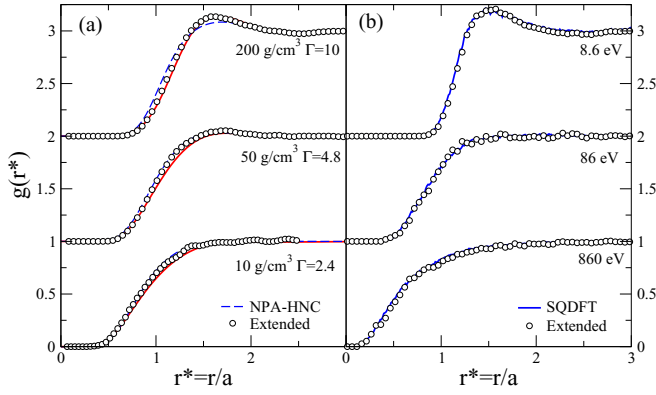


FIG. 4. (a) Pair distribution of carbon at 100 eV and for densities of 200 (top), 50 (middle), and 10 g/cm³ (bottom). The open black circles are EXT. FPMD simulations; dashed blue lines: NPA-HNC results and heavy solid red lines: the effective OCP with Γ given in Table I. (b) Same for carbon at 10 g/cm³ and for temperatures of 0.1 (top), 1 (middle), and 10 MK (bottom), computed with the EXT. FPMD model (open circles) and with SQDFT simulations (solid blue line).

kinetic and the degenerate regime. We will thus address this particular isochor in the next section.

VI. IONIZATION ALONG AN ISOCHOR

Recently, Bethkenhagen *et al.* [16], using the spectral quadrature DFT method (SQDFT), produced extensive simulations of 64 atoms of carbon along the 10 g/cm³ isochor for temperatures ranging from 0.1 to 10 MK (8.6 to 862 eV). In

this case, the system then goes from a degenerate state at low temperature to an ideal state at high temperature (see Table II).

We first used the pressure given by the simulation to get an estimation of the ionization Q_P as reported in Table II. We then used the PDFs produced by the simulation to apply the effective OCP method. Figure 5(a) displays the comparison of the simulation data with the best OCP fit for the whole range of temperatures. We get a very good overall agreement, except at low temperature ($0.86 < T < 86$ eV) for which we observe a bump before the one given by the OCP model. This feature is attributed, as in the previous case, to the onset of binding and to the tendency of carbon to form (potentially short-lived) dimers and more complex structures. Beyond 86 eV the agreement becomes really very good and allows for the definition of an unambiguous eOCP coupling parameter from which we get a structural Q_S ionization reported in Table II.

The corresponding SSFs are shown in Fig. 5(b) and, as for the isotherm case, exhibit the expected disagreement with the eOCP at vanishing wave number. This behavior is restituted by the screened formula (heavy solid blue line) with screening parameters given in Table II.

To check the compatibility of SQDFT with our EXT. FPMD simulations, we compare in Fig. 4(b) the PDFs produced by both approaches for 10 g/cm³ and 0.1, 1, and 10 MK (8.62, 86.2, and 862 eV). The agreement is quite good and confirms that the disagreement with the effective OCP at 0.1 MK cannot be attributed to the computational approach. The pressures given by the EXT. FPMD simulations are respectively, 4 450, 32 820, and 471 200 Gpa, in excellent agreement with SQDFT pressures given in Table II.

We have gathered in Fig. 6 and in Table II our predictions for the ionization of carbon along the 10 g/cm³ isochor. We

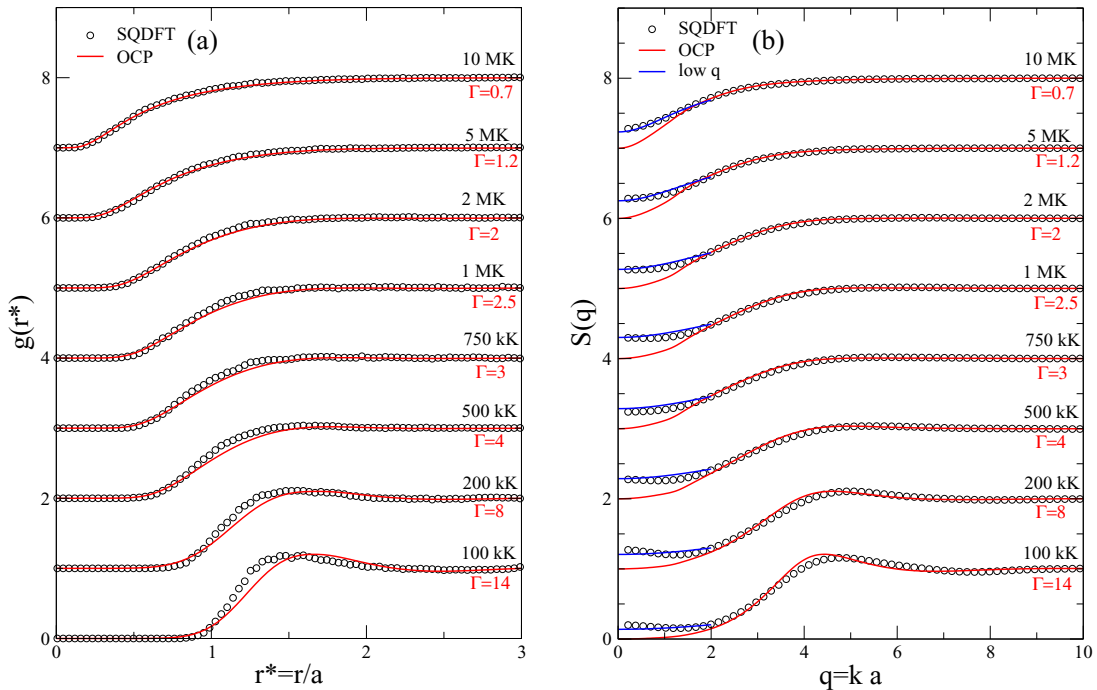


FIG. 5. PDF (a) and static structure factor (b) of carbon along the 10 g/cm³ isochor and for temperatures of 8.6, 17.2, 43.1, 64.6, 86.2, 174.4 31.0, and 862 eV computed with the SQDFT simulations (open black circles) and matched with the OCP one (heavy red line). The blue line in (b) is the low q expansion of the SSF for screened systems.

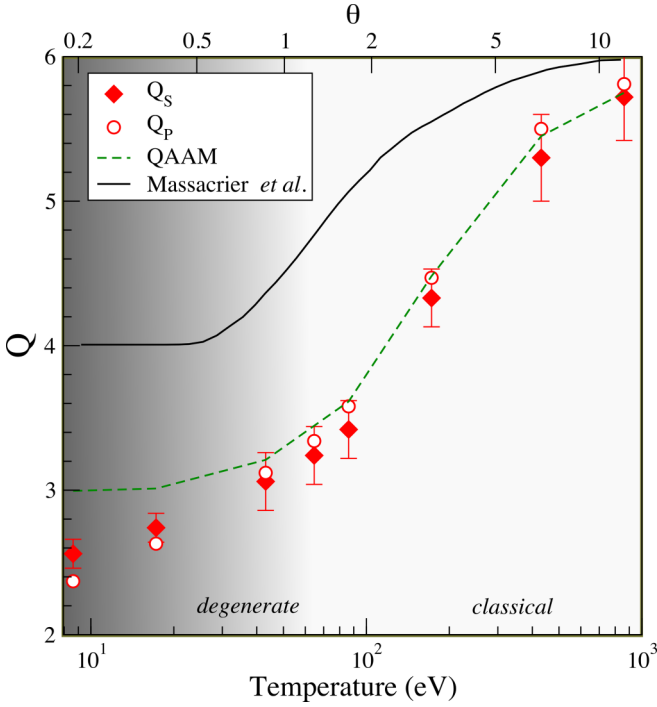


FIG. 6. Ionization versus temperature along the 10 g/cm^3 carbon isochor. Red diamonds with errors bars are the structure estimation Q_S , and red circles the pressure estimation Q_P , both from SQDFT simulations [16]. The green dashed and the solid black lines are, respectively, the QAAM [8] and the Massacrier *et al.* estimations [33].

note again the equivalence between the two definitions of the ionization. The error bars on Q_S are deduced from an error of 20% on the effective coupling parameter.

The agreement with the QAAM code is good except for the two lowest temperatures for which QAAM predicts slightly higher ionization ($\simeq 5\%$). In this region a strong departure from the eOCP is observed which we will quantify in the next section. For comparison, we have also added the prediction of Massacrier *et al.* [33], which is significantly higher ($\simeq 20\%$).

VII. NON-OCP BEHAVIOR

As shown from Figs. 3 and 6 and from Tables I and II, ionizations obtained by the pressure or by the structure are equivalent. These latter being defined by an adjustment *by eye*, it would be interesting to introduce a more systematic definition. This is done by taking the pressure ionization Q_P and by deducing the corresponding coupling parameter $\Gamma_P = Q_P^2/aT$ which is very close to the previous Γ (see Tables I and II). We thus can define unambiguously an effective OCP through the ionization given by the pressure. The coupling values are nearly identical to the effective coupling leading to a PDF almost indistinguishable from the previous one obtained by the fitting process. We can now quantify the mismatch between the simulated and the OCP PDFs. We define a non-OCP behavior by

$$\Delta_{\text{NO}} = \sum_i [g_i(r_i) - g_{\text{OCP}}(r_i)]^2 r_i^2. \quad (6)$$

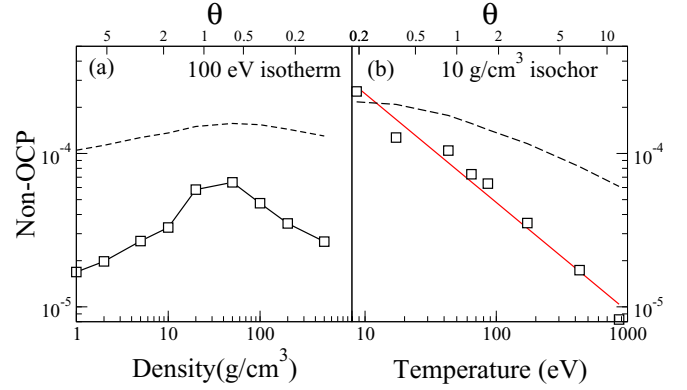


FIG. 7. Non-OCP behavior along, (a): the 100 eV isotherm, and (b): the 10 g/cm^3 isochor. The dashed line represents the finite temperature inverse screening length divided by 10^4 and the red line a power law $x^{-0.7}$.

The summation is restricted to the largest distance $L/2$, where L is the length of the box in a units, explored when computing the $g(r)$ in a simulation of N atoms ($L/a = (4\pi/3)^{1/3}N^{1/3} = 1.612N^{1/3}$). The lower this parameter, the closer to a pure OCP the system is. We have represented Δ_{NO} in Fig. 7 along the 100 eV carbon isotherm (a) and along the 10 g/cm^3 carbon isochor (b). Along the isochor, the situation is rather simple: the higher the temperature, the lower is this parameter, i.e., the closer to a pure OCP the system is. In the range of temperatures Δ_{NO} scales as $\propto T^{-0.7}$ [red line in Fig. 7(b)] and is coherent with a decreasing screening parameter κ (dashed line). Along the 100 eV isotherm, the situation is more complex: Δ_{NO} first increases up to density of about 50 g/cm^3 and after decreases with the density, with no clear scaling. Along the isotherm, the screening parameter κ is almost constant.

VIII. CONCLUSION

We have proposed an alternative definition of the ionization in the hot dense regime, based on molecular dynamics simulations in the DFT framework. More precisely, using the EXT. FPMD method, we have produced molecular dynamics simulations along the 100 eV carbon isotherm, from which we have extracted ionizations either from the total pressure or from the structure by matching the PDFs with an eOCP. These two equivalent points of view are leading to evaluation of the ionization consistent with previous PURGATORIO and QAAM estimations. We have also tested our approach along the 10 g/cm^3 carbon isochor with a completely different approach (SQDFT) and found the same equivalence between pressure and structure defined ionization, still in agreement with AA models. Finally, when this equivalence no longer works, at low temperature or intermediate degeneracy, we propose a parameter that measures the tendency of the system to form bonds and complex structures (dimers, polymers).

We believe that this eOCP technique could be used in experiments to extract an average ionization from the Fourier transform of an x-ray diffraction image of the plasma which shows the static structure factor [39].

ACKNOWLEDGMENTS

C. Dharma-Wardana is warmly acknowledged for providing his NPA-HNC data on pair correlation functions.

APPENDIX A: THE EXT. FPMD METHOD

Running simulations for carbon along the 100 eV isotherm, between 1 and 500 g/cm³ is rather challenging. As said before, we must be able to handle simulations in a kinetic regime ($\theta = 8$) at low density and in an almost fully degenerate regime ($\theta = 0.1$) at high density (see Table I). In the first case the difficulty arises from the huge number of orbitals to consider. We can see in Table I, that up to 48 100 orbitals are needed for a 64-atom system at the lowest density of 1 g/cm³ under the constraint of a minimum occupation of 10^{-4} . At high density, if the simulation becomes much easier, due to the low number of orbitals, special care must be brought to the pseudopotential to avoid overlap occurrences and to allow for an almost full ionization which supposes an all-electrons pseudopotential.

To circumvent these, the constraints we used the recently implemented the EXT. FPMD option [40] in ABINIT to produce KS-DFT molecular dynamics of hot systems in an economic way. Instead of considering a number of orbitals adapted to the density as reported in Table I, which depends on the degeneracy parameter θ and on the minimum occupation [41], we used a fixed number of 500 orbitals for the whole range of densities with a constant number of 64 ions.

This economy is made possible by considering only active orbitals that are involved in bound/free processes for electrons. Orbitals of higher energy are left and replaced by a free electron gas description whose density of states is shifted by an energy U_0 as evidenced by Zhang *et al.* [42]. This approach should not be confused with the orbital free molecular dynamics method (OFMD [43]), since, even at very high temperatures, inner core orbitals are preserved. It is the ionization of 1s states that drives the maximum of shock compressibility curve (the Hugoniot), which turns out to be different from the one obtained by OFMD simulations.

In the EXT. FPMD approach, all contributions are split in two parts. For example, the kinetic energy contribution reads

$$E_K = - \sum_{i=1}^{N_c} f_n \langle \psi_i | \nabla^2 | \psi_i \rangle + 2 \int_{N_c}^{\infty} f_n \epsilon_n^{\text{FG}} dn, \quad (\text{A1})$$

where the discrete summation is made on the N_c Kohn-Sham orbitals ψ_i explicitly kept in the calculation (here 500), and the second part involves the electron gas energy $\epsilon_n^{\text{FG}} = 1/2(6\pi^2 n/\Omega)^{2/3}$ of the n^{th} (singly occupied) orbital, Ω is the volume, $\beta = 1/k_B T$ is the temperature, μ is the chemical potential, and $f_n = (e^{\beta(\epsilon_n^{\text{FG}} + U_0 - \mu)} + 1)^{-1}$ is the Fermi-Dirac occupation (shifted by U_0). There are different strategies to set the shift in energy U_0 and we choose to average the potential energy in the whole box of simulation [40].

All contributions are corrected by the corresponding electron gas formulations and are analytical. The kinetic energy contribution is given by

$$E_K^{\text{FG}} = \frac{\sqrt{2}}{\pi^2} \frac{\Omega}{\beta^{5/2}} \mathcal{F}_{\frac{3}{2}}(\gamma, \beta \epsilon_{N_c}^{\text{FG}}), \quad (\text{A2})$$

where $\gamma = \beta(\mu - U_0)$ and $\mathcal{F}_{\frac{3}{2}}(\gamma, \bar{n})$ is the incomplete Fermi integral of order $3/2$

$$\mathcal{F}_{\frac{3}{2}}(a, b) = \int_b^{\infty} \frac{x^{3/2}}{e^{x-a} + 1} dx, \quad (\text{A3})$$

with the lower bound $b = \beta \epsilon_{N_c}^{\text{FG}}$ and $a = \gamma$. Improved analytical expressions for Fermi integrals (complete and incomplete) can be found in Ref. [44].

Similarly, the number of electrons reads

$$N_e^{\text{FG}} = \frac{\sqrt{2}}{\pi^2} \frac{\Omega}{\beta^{3/2}} \mathcal{F}_{\frac{1}{2}}(\gamma, \beta \epsilon_{N_c}^{\text{FG}}). \quad (\text{A4})$$

The correction to the stress tensor is straightforward.

$$\sigma_{\alpha\beta}^{\text{FG}} = -\frac{2}{3\Omega} \delta_{\alpha\beta} E_K^{\text{FG}}. \quad (\text{A5})$$

The correction on the electronic pressure will automatically follow as it is proportional to the trace of the stress tensor $P = -\sigma_{ii}/3$, and is obviously computed after we have added the Fermi gas contributions to the stresses.

APPENDIX B: SPECTRAL QUADRATURE (SQ) METHOD

The spectral quadrature (SQ) method [45] is a density-matrix based $O(N)$ method for the solution of the Kohn-Sham equations that is particularly well suited for calculations at high temperature. In the SQ method, all quantities of interest, such as energies, forces, and stresses, are expressed as bilinear forms or sums of bilinear forms which are then approximated by quadrature rules that remain spatially localized by exploiting the locality of electronic interactions in real space [46], i.e., the exponential decay of the density matrix at finite temperature [47–50]. In the absence of truncation, the method becomes mathematically equivalent to the recursion method [51,52] for the choice of Gauss quadrature, while for Clenshaw-Curtis quadrature, the classical Fermi operator expansion (FOE) [53,54] in Chebyshev polynomials is recovered. Being formulated in terms of the finite-temperature density matrix, the method is applicable to metallic and insulating systems alike, with increasing efficiency at higher temperature as the Fermi operator becomes smoother and the density matrix becomes more localized [55]. $O(N)$ scaling is obtained by exploiting the locality of the density matrix at finite temperature, while the exact diagonalization limit is obtained to desired accuracy with increasing quadrature order and localization radius. Convergence to standard $O(N^3)$ plane-wave results, for metallic and insulating systems alike, is readily obtained [55,56].

While mathematically equivalent to classical FOE methods in the absence of truncation for a particular choice of quadrature, the more general SQ formulation affords a number of advantages in practice [55,56]. These include: (1) The method is expected to be more robust since it explicitly accounts for the effect of truncation on the Chebyshev expansion. (2) The method computes only the elements of the density matrix needed to evaluate quantities of interest—e.g., only diagonal elements to obtain densities and energies—rather than computing the full density matrix (to specified threshold) as in FOE methods. (3) The method computes the Fermi

energy without storage or recomputation of Chebyshev matrices as required in FOE methods. (4) The method admits a decomposition of the global Hamiltonian into local sub-Hamiltonians in real space, reducing key computations to local sub-Hamiltonian matrix-vector multiplies rather than global full-Hamiltonian matrix-matrix multiplies as in FOE methods. Since the associated local multiplies are small (according to the decay of the density matrix) and independent of one another, the method is particularly well suited to massively parallel implementation; whereas the global sparse matrix-matrix multiplies required in FOE methods pose significant challenges for parallel implementation [57].

APPENDIX C: QAAM CODE

The nonrelativistic version of the quantum average-atom model QAAM is used [8]. QAAM is based on the muffin-tin approximation to describe the electronic structure. Assuming that the electrons are in local thermodynamic equilibrium at the temperature T_e and using the finite-temperature density-functional-theory in the local density approximation [58–60], the average-atom equations reads

$$[-\hbar^2/(2m_e)\nabla^2 + V_{ie}(r)]\psi_a(r) = \epsilon_a\psi_a(r), \quad (C1)$$

where \hbar is the reduced Planck constant, m_e is the electron rest mass, and ϵ_a a one-electron energy. $a \equiv n\ell$ for the bound states and $a \equiv \epsilon\ell$ for the continuum states, where $n(\ell)$ is the principal (orbital) quantum number. $V_{ie}(r)$ is the Kohn-Sham potential

$$V_{ie}(r) = -\frac{Z_e^2}{r} + e^2 \int dr' \frac{n_e(r')}{|r-r'|} + V_{xc}(r), \quad (C2)$$

where e is the elementary charge and Z is the nuclear charge. $V_{xc}(r)$ is the finite-temperature exchange-correlation potential [61]. The one-electron wave function

$$\psi_a(r) = \frac{P_a(r)}{r} Y_{\ell_a, m_{\ell_a}}(\theta, \phi) \chi_{m_s}(\sigma) \quad (C3)$$

introduces the spherical harmonics $Y_{\ell, m}(\theta, \phi)$ and the spin function $\chi_{m_s}(\sigma)$. The bound and continuum wave functions are normalized such that $\int_0^{+\infty} dr P_{n\ell}(r) P_{n'\ell}(r) = \delta_{nn'}$ and $\int_0^{+\infty} dr P_{\epsilon\ell}(r) P_{\epsilon'\ell}(r) = \delta(\epsilon - \epsilon')$.

The total electron density is $n_e(r) = n_{e,b}(r) + n_{e,f}(r)$, where

$$n_{e,b}(r) = \frac{1}{4\pi r^2} \sum_{n\ell} f(\epsilon_{n\ell}, \mu, T_e) D_{\ell} P_{n\ell}(r)^2$$

and

$$n_{e,f}(r) = \frac{1}{4\pi r^2} \sum_l \int_0^{+\infty} d\epsilon f(\epsilon, \mu, T_e) D_{\ell} P_{\epsilon\ell}(r)^2.$$

$D_{\ell} = 4\ell + 2$ and $f(x, \mu, T_e) = [1 + e^{(x-\mu)/k_B T_e}]^{-1}$ is the Fermi-Dirac distribution function. μ is the chemical potential determined such that $\int_0^a dr 4\pi r^2 n_e(r) = Z$, where a is the previously defined Wigner-Seitz radius (see Sec. I). Assuming that $V_{ie}(r) = 0$ for $r \geq a$, the wave functions and the Kohn-Sham potential are self-consistently computed. Concerning the bound states, principal quantum number values up to 15 can be considered. Concerning the continuum states, the maximum orbital quantum number ℓ_{\max} is set equal to 15. Following Blenski and Ishikawa [62], the contribution of orbital quantum number higher than ℓ_{\max} is evaluated using a well-known sum rule obeyed by the Bessel functions. Once the self-consistent process complete, the average ionization Q is evaluated using $Q = \frac{4\pi}{3} a^3 n_e(a)$ [63].

-
- [1] A. L. Kritcher, D. C. Swift, T. Doepfner, B. Bachmann, L. X. Benedict, G. W. Collins, J. L. DuBois, F. Elsner, G. Fontaine, J. A. Gaffney, A. Hamel, S. Lazicki, W. R. Johnson, N. Kostinski, D. Kraus, M. J. MacDonald, B. Maddox, M. E. Martin, P. Neumayer, A. Nikroo *et al.*, A measurement of the equation of state of carbon envelopes of white dwarfs, *Nature (London)* **584**, 51 (2020).
- [2] I. Krisch and H. J. Kunze, Measurements of electrical conductivity and the mean ionization state of nonideal aluminium plasma, *Phys. Rev. E* **58**, 6557 (1998).
- [3] P. Renaudin, V. Recoules, P. Noiret, and J. Cl  rouin, Electronic structure and equation of state data of warm dense gold, *Phys. Rev. E* **73**, 056403 (2006).
- [4] X. Gonze, B. Amadon, G. Antonius, F. Arnardi, L. Baguet, J.-M. Beuken, J. Bieder, F. Bottin, J. Bouchet, E. Bousquet, N. Brouwer, F. Bruneval, G. Brunin, T. Cavignac, J.-B. Charraud, W. Chen, M. C  t  , S. Cottenier, J. Denier, G. Geneste, P. Ghosez, M. Giantomassi, Y. Gillet, O. Gingras, D. R. Hamann, G. Hautier, X. He, N. Helbig, N. Holzwarth, Y. Jia, F. Jollet, W. Lafargue-Dit-Hauret, K. Lejaeghere, M. A. L. Marques, A. Martin, C. Martins, H. P. C. Miranda, F. Naccarato, K. Persson, G. Petretto, V. Planes, Y. Pouillon, S. Prokhorenko, F. Ricci, G.-M. Rignanese, A. H. Romero, M. M. Schmitt, M. Torrent, M. J. van Setten, B. Van Troeye, M. J. Verstraete, G. Z  rah, and J. W. Zwanziger, The abinitproject: Impact, environment and recent developments, *Comput. Phys. Commun.* **248**, 107042, (2020).
- [5] K. P. Driver, F. Soubiran, and B. Militzer, Path integral Monte Carlo simulations of warm dense aluminum, *Phys. Rev. E* **97**, 063207 (2018).
- [6] M. Bethkenhagen, B. B. L. Witte, M. Sch  rner, G. R  pke, T. D  ppner, D. Kraus, S. H. Glenzer, P. A. Sterne, and R. Redmer, Carbon ionization at gigabar pressures: An ab initio perspective on astrophysical high-density plasmas, *Phys. Rev. Res.* **2**, 023260 (2020).
- [7] P. A. Sterne, S. B. Hansen, B. G. Wilson, and W. A. Isaacs, Equation of state, occupation probabilities and conductivities in the average atom Purgatorio code, *High Energy Density Phys.* **3**, 278 (2007).
- [8] G. Faussurier, C. Blancard, and M. Bethkenhagen, Carbon ionization from a quantum average-atom model up to gigabar pressures, *Phys. Rev. E* **104**, 025209 (2021).
- [9] M. W. C. Dharma-wardana, Ionization of carbon at 10–100 times the diamond density and in the 10⁶ k temperature range, *Phys. Rev. E* **104**, 015201 (2021).

- [10] M. S. Murillo, J. Weisheit, S. B. Hansen, and M. W. C. Dharma-wardana, Partial ionization in dense plasmas: Comparisons among average-atom density functionals models, *Phys. Rev. E* **87**, 063113 (2013).
- [11] W. L. Slattery, G. D. Doolen, and H. E. DeWitt, Improved equation of state for the classical one-component plasma, *Phys. Rev. A* **21**, 2087 (1980).
- [12] N. Desbiens, P. Arnault, and J. Clérouin, Parametrization of pair correlation function and static structure factor of the one component plasma across coupling regimes, *Phys. Plasmas* **23**, 092120 (2016).
- [13] J. Daligault, Liquid-State Properties of a One-Component Plasma, *Phys. Rev. Lett.* **96**, 065003 (2006).
- [14] M. Zaghoo, T. R. Boehly, J. R. Rygg, P. M. Celliers, S. X. Hu, and G. W. Collins, Breakdown of Fermi Degeneracy in the Simplest Liquid Metal, *Phys. Rev. Lett.* **122**, 085001 (2019).
- [15] M. W. C. Dharma-Wardana and R. Taylor, Exchange and correlation potentials for finite temperature quantum calculations at intermediate degeneracies, *J. Phys. C* **14**, 629 (1981).
- [16] M. Bethkenhagen, A. Sharma, P. Suryanarayana, J. E. Pask, B. Sadigh, and S. Hamel, Thermodynamic, structural, and transport properties of dense carbon up to 10 million Kelvin from Kohn-Sham density functional theory calculations, [arXiv:2110.01034](https://arxiv.org/abs/2110.01034) (2021).
- [17] C. E. Starrett, N. M. Gill, T. Sjostrom, and C. W. Greeff, Wide ranging equation of state with Tartarus: A hybrid Green's function/orbital based average atom code, *Comput. Phys. Commun.* **235**, 50 (2019).
- [18] T. J. Callow, S. B. Hansen, E. Krausler, and A. Cangi, First-principles derivation and properties of density-functional average-atom models, *Phys. Rev. Res.* **4**, 023055 (2022).
- [19] G. Massacrier, M. Böhme, J. Vorberger, F. Soubiran, and B. Militzer, Reconciling ionization energies and band gaps of warm dense matter derived with *ab initio* simulations and average atom models, *Phys. Rev. Res.* **3**, 023026 (2021).
- [20] C. Blancard and G. Faussurier, Equation of state and transport coefficients for dense plasmas, *Phys. Rev. E* **69**, 016409 (2004).
- [21] G. Faussurier, C. Blancard, P. Cossé, and P. Renaudin, Equation of state, transport coefficients, and stopping power of dense plasmas from the average-atom model self-consistent approach for astrophysical and laboratory plasmas, *Phys. Plasmas* **17**, 052707 (2010).
- [22] G. Miloshevsky and A. Hassanein, Atomic and optical properties of warm dense copper, *Phys. Rev. E* **92**, 033109 (2015).
- [23] A. F. Nikiforov, V. G. Novikov, and V. B. Uvarov, *Quantum-Statistical Models of Hot Dense Matter* (Birkhäuser, Basel, 2005).
- [24] J. Clérouin, G. Robert, P. Arnault, C. Ticknor, J. D. Kress, and L. A. Collins, Evidence for out-of-equilibrium states in warm dense matter probed by x-ray Thomson scattering, *Phys. Rev. E* **91**, 011101(R) (2015).
- [25] Y. Hou, Y. Fu, R. Bredow, D. Kang, R. Redmer, and J. Yuan, Average-atom model for two-temperature states and ionic transport properties of aluminum in the warm dense matter regime, *High Energy Density Phys.* **22**, 21 (2017).
- [26] J. Clérouin, G. Robert, P. Arnault, J. D. Kress, and L. A. Collins, Behavior of the coupling parameter under isochoric heating in a high-Z plasma, *Phys. Rev. E* **87**, 061101(R) (2013).
- [27] Z.-Q. Wang, J. Tang, Y. Hou, Q.-F. Chen, X.-R. Chen, J.-Y. Dai, X.-J. Meng, Y.-J. Gu, L. Liu, G.-J. Li, Y.-S. Lan, and Z.-G. Li, Benchmarking the effective one-component plasma model for warm dense neon and krypton within quantum molecular dynamics simulation, *Phys. Rev. E* **101**, 023302 (2020).
- [28] Y. Hou, Y. Jin, P. Zhang, D. Kang, C. Gao, R. Redmer, and J. Yuan, Ionic self-diffusion coefficient and shear viscosity of high-z materials in the hot dense regime, *Matter Radiat. Extremes* **6**, 026901 (2021).
- [29] A. Blanchet, F. Soubiran, M. Torrent, and J. Clérouin, Extended first-principles molecular dynamics simulations of hot dense boron: Equation of state and ionization, *Contrib. Plasma Phys.*, e202100234 (2022).
- [30] J. Clérouin, P. Arnault, C. Ticknor, J. D. Kress, and L. A. Collins, Unified Concept of Effective One Component Plasma for Hot Dense Plasmas, *Phys. Rev. Lett.* **116**, 115003 (2016).
- [31] T. Ott, M. Bonitz, L. G. Stanton, and M. S. Murillo, Coupling strength in Coulomb and Yukawa one-component plasmas, *Phys. Plasmas* **21**, 113704 (2014).
- [32] H. Y. Sun, D. Kang, Y. Hou, and J. Y. Dai, Transport properties of warm and hot dense iron from orbital free and corrected Yukawa potential molecular dynamics, *Matter Radiat. Extremes* **2**, 287 (2017).
- [33] G. Massacrier, A. Y. Potekhin, and G. Chabrier, Equation of state for partially ionized carbon and oxygen mixtures at high temperatures, *Phys. Rev. E* **84**, 056406 (2011).
- [34] J. P. Perdew, K. Burke, and M. Ernzerhof, Generalized Gradient Approximation Made Simple, *Phys. Rev. Lett.* **77**, 3865 (1996).
- [35] N. A. W. Holzwarth, A. R. Tackett, and G. E. Matthews, A projector augmented wave (PAW) code for electronic structure calculations, part I: Atompaw for generating atom-centered functions, *Comput. Phys. Commun.* **135**, 329 (2001).
- [36] P. Blaha, K. Schwarz, F. Tran, R. Laskowski, G. K. H. Madsen, and L. D. Marks, WIEN2k: An APW+lo program for calculating the properties of solids, *J. Chem. Phys.* **152**, 074101 (2020).
- [37] K. Lejaeghere, V. Van Speybroeck, G. Van Oost, and S. Cottenier, Error estimates for solid-state density-functional theory predictions: An overview by means of the ground-state elemental crystals, *Crit. Rev. Solid State Mater. Sci.* **39**, 1 (2014).
- [38] A similar agreement between QMD static structure factor and effective OCP of carbon at 100 eV and 50 g/cm³ is shown in Fig. 5 of Ref. [8]. Note that the abscissa of OCP being in *a* units, the one of QMD simulations must be multiplied by 0.863 (Wigner-Seitz radius for 50 g/cm³) to get a perfect agreement.
- [39] D. Riley, N. C. Woolsey, D. McSherry, I. Weaver, A. Djaoui, and E. Nardi, X-Ray Diffraction from a Dense Plasma, *Phys. Rev. Lett.* **84**, 1704 (2000).
- [40] A. Blanchet, J. Clérouin, M. Torrent, and F. Soubiran, Extended FPMD model for high temperatures ranges simulations in Abinit: Application to warm dense aluminum, *Comput. Phys. Commun.* **271**, 108215 (2022).
- [41] A. Blanchet, M. Torrent, and J. Clérouin, Requirements for very high temperature Kohn-Sham DFT simulations and how to bypass them, *Phys. Plasmas* **27**, 122706 (2020).
- [42] S. Zhang, H. Wang, W. Kang, P. Zhang, and X. T. He, Extended application of Kohn-Sham first-principles molecular dynamics method with plane wave approximation at high energy—from cold materials to hot dense plasmas, *Phys. Plasmas* **23**, 042707 (2016).

- [43] F. Lambert, J. Cl rouin, S. Mazevet, and D. Gilles, Properties of hot dense plasmas by orbital-free molecular dynamics, *Contrib. Plasma Phys.* **47**, 272 (2007).
- [44] V. V. Karasiev, D. Chakraborty, and S. B. Trickey, Improved analytical representation of combinations of Fermi-Dirac integrals for finite-temperature density functional calculations, *Comput. Phys. Commun.* **192**, 114 (2015).
- [45] P. Suryanarayana, On spectral quadrature for linear-scaling density functional theory, *Chem. Phys. Lett.* **584**, 182 (2013).
- [46] E. Prodan and W. Kohn, Nearsightedness of electronic matter, *Proc. Natl. Acad. Sci.* **102**, 11635 (2005).
- [47] S. Goedecker, Decay properties of the finite-temperature density matrix in metals, *Phys. Rev. B* **58**, 3501 (1998).
- [48] S. Ismail-Beigi and T. A. Arias, Locality of the Density Matrix in Metals, Semiconductors, and Insulators, *Phys. Rev. Lett.* **82**, 2127 (1999).
- [49] M. Benzi, P. Boito, and N. Razouk, Decay properties of spectral projectors with applications to electronic structure, *SIAM Rev.* **55**, 3 (2013).
- [50] P. Suryanarayana, On nearsightedness in metallic systems for $O(N)$ density functional theory calculations: A case study on aluminum, *Chem. Phys. Lett.* **679**, 146 (2017).
- [51] R. Haydock, V. Heine, and M. J. Kelly, Electronic-structure based on local atomic environment for tight-binding bands, *J. Phys. C* **5**, 2845 (1972).
- [52] R. Haydock, V. Heine, and M. J. Kelly, Electronic-structure based on local atomic environment for tight-binding bands: II, *J. Phys. C* **8**, 2591 (1975).
- [53] S. Goedecker and L. Colombo, Efficient Linear Scaling Algorithm for Tight-Binding Molecular Dynamics, *Phys. Rev. Lett.* **73**, 122 (1994).
- [54] S. Goedecker and M. Teter, Tight-binding electronic-structure calculations and tight-binding molecular dynamics with localized orbitals, *Phys. Rev. B* **51**, 9455 (1995).
- [55] P. P. Pratapa, P. Suryanarayana, and J. E. Pask, Spectral quadrature method for accurate $O(N)$ electronic structure calculations of metals and insulators, *Comput. Phys. Commun.* **200**, 96 (2016).
- [56] P. Suryanarayana, P. P. Pratapa, A. Sharma, and J. E. Pask, SQDFT: Spectral Quadrature method for large-scale parallel $O(N)$ Kohn-Sham calculations at high temperature, *Comput. Phys. Commun.* **224**, 288 (2018).
- [57] D. R. Bowler and T. Miyazaki, $O(N)$ methods in electronic structure calculations, *Rep. Prog. Phys.* **75**, 036503 (2012).
- [58] P. Hohenberg and W. Kohn, Inhomogeneous electron gas, *Phys. Rev.* **136**, B864 (1964).
- [59] W. Kohn and L. J. Sham, Self-consistent equations including exchange and correlation, *Phys. Rev.* **140**, A1133 (1965).
- [60] N. D. Mermin, Thermal properties of the inhomogeneous electron gas, *Phys. Rev.* **137**, A1441 (1965).
- [61] S. Ichimaru, H. Iyetomi, and S. Tanaka, Statistical physics of dense plasmas: Thermodynamics, transport coefficients and dynamic correlations, *Phys. Rep.* **149**, 91 (1987).
- [62] T. Blenski and K. Ishikawa, Pressure ionization in the spherical ion-cell model of dense plasmas and a pressure formula in the relativistic Pauli approximation, *Phys. Rev. E* **51**, 4869 (1995).
- [63] R. M. More, Pressure ionization resonances, and the continuity of bound and free states, in *Advances in Atomic and Molecular Physics* (Academic, New York, 1985), Vol. 21, pp. 305–355d.